frontiers | Frontiers in Physiology

TYPE Original Research
PUBLISHED 21 August 2023
DOI 10.3389/fphys.2023.1195502

OPEN ACCESS

EDITED BY
Guangyu Zhu,
Xi'an Jiaotong University, China

REVIEWED BY
Jan Christoph,
University of California, San Francisco, United States
Shengzhang Wang,
Fudan University, China

*CORRESPONDENCE
Yong Wang,
yong.wang@ds.mpg.de

†These authors have contributed equally to this work

RECEIVED 28 March 2023
ACCEPTED 31 July 2023
PUBLISHED 21 August 2023

CITATION
Zhang Y, Kalhöfer-Köchling M, Bodenschatz E and Wang Y (2023), Physical model of end-diastolic and end-systolic pressure-volume relationships of a heart.
Front. Physiol. 14:1195502.
doi: 10.3389/fphys.2023.1195502

Physical model of end-diastolic and end-systolic pressure-volume relationships of a heart

Yunxiao Zhang[1,2†], Moritz Kalhöfer-Köchling[1,2†], Eberhard Bodenschatz[1,2,3,4] and Yong Wang[1,2*]

[1]Laboratory for Fluid Physics, Pattern Formation and Biocomplexity, Max Planck Institute for Dynamics and Self-Organization, Göttingen, Germany, [2]DZHK (German Center for Cardiovascular Research), Partner Site Göttingen, Göttingen, Germany, [3]Institute for Dynamics of Complex Systems, University of Göttingen, Göttingen, Germany, [4]Laboratory of Atomic and Solid-State Physics and Sibley School of Mechanical and Aerospace Engineering, Cornell University, Ithaca, NY, United States

Left ventricular stiffness and contractility, characterized by the end-diastolic pressure-volume relationship (EDPVR) and the end-systolic pressure-volume relationship (ESPVR), are two important indicators of the performance of the human heart. Although much research has been conducted on EDPVR and ESPVR, no model with physically interpretable parameters combining both relationships has been presented, thereby impairing the understanding of cardiac physiology and pathology. Here, we present a model that evaluates both EDPVR and ESPVR with physical interpretations of the parameters in a unified framework. Our physics-based model fits the available experimental data and *in silico* results very well and outperforms existing models. With prescribed parameters, the new model is used to predict the pressure-volume relationships of the left ventricle. Our model provides a deeper understanding of cardiac mechanics and thus will have applications in cardiac research and clinical medicine.

KEYWORDS

cardiac mechanics, end-diastolic pressure-volume relationship, end-systolic pressure-volume relationship, left ventricle, physics-based model

1 Introduction

A well-functioning heart is critical to the quality of human life (Gilbert et al., 2007). The pump function of the heart can be captured by the pressure-volume (PV) loop, which is a simple and useful framework for analyzing cardiac mechanics from a physical perspective (Witzenburg et al., 2017). Deoxygenated blood is pumped from the right ventricle (RV) to the lungs, and in turn, oxygenated blood is pumped from the left ventricle (LV) to the rest of the body. Because the LV is physically subjected to more stress and strain than the RV, left-sided heart failure is more common than right-sided or biventricular heart failure (MedlinePlus, 2023), wherefore we have focused our analysis on the LV. The concept, however, can be applied to the RV likewise.

As shown in Figure 1, exemplary for a PV loop, the lower right point (point 1) indicates the end-diastolic (ED) state of the LV. Varying ED filling pressures

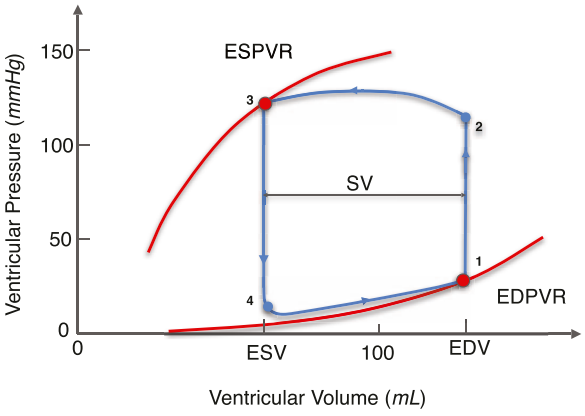

FIGURE 1
Illustration of the PV loop, ESPVR, and EDPVR of the LV. The EDPVR and ESPVR are highlighted in red and the PV loop is in blue. The arrows on the PV loop correspond to the direction of the LV beating cycle. Curve 3-4-1 corresponds to the diastolic phase. At point 1, the ventricular volume reaches its maximum value as the blood fills into the LV, which is called the EDV. Similarly, curve 1-2-3 corresponds to the systolic phase. At point 3, the ventricular volume reaches its minimum value during LV contraction, which is referred to as ESV. The difference between EDV and ESV is the SV, indicating the amount of blood pumped by the LV per cardiac cycle. At different filling pressure and contractility, points 1 and 3 move on a single curve called the EDPVR and ESPVR, respectively. (EDPVR, end-diastolic pressure-volume relationship; ESPVR: end-systolic pressure-volume relationship; EDV, end-diastolic volume; ESV, end-systolic volume; SV, stroke volume).

yields a change in ED volume. For a heart, these data points fall roughly on a single curve which is termed the end-diastolic pressure-volume relationship (EDPVR) (Sunagawa et al., 1983). The EDPVR is widely used to estimate the mechanical property of myocardium (Ten Brinke et al., 2010; Krishnamurthy et al., 2013a; Dabiri et al., 2018; Palit et al., 2018). The upper left point (point 3) on the PV loop indicates the end-systolic (ES) state of the LV, and the related curve is the end-systolic pressure-volume relationship (ESPVR). The ESPVR and its slope are generally used to describe the contractility of the heart. In this work we present a physics-based model for both the EDPVR and ESPVR.

The EDPVR comprises a number of important markers used by both researchers and clinicians in health assessments. Many studies have shown that the EDPVR has a strong association with heart diseases. Despite its long history, the EDPVR continues to gain increased attention. Goto et al. (1985) studied the effects of right ventricular ischemia on LV EDPVR in canine hearts. A leftward and upward shift in the LV EDPVR was observed with no change in LV myocardial performance. Ten Brinke et al. (2010) predicted the LV EDPVR in patients with end-stage heart failure (LV ejection fraction <40%) using single-beat estimation and concluded that such method facilitated less invasive EDPVR estimation. Schwarzl et al. (2016) showed that, due to LV remodeling, the EDPVR was shifted rightward and leftward in heart failures with reduced ejection fraction and heart failure with preserved ejection fraction, respectively, compared with the reference case. In addition, the risk of heart failure for non-heart failure individuals was found to be associated with the changes in LV capacitance and stiffness, which can be extracted from the EDPVR. Witzenburg and Holmes (Witzenburg et al., 2017) stated that EDPVR contains information not only about the mechanical properties of the myocardium but also about LV geometry. Since cardiac diseases alter the shape or stiffness of the heart and thus the EDPVR, the EDPVR is important and helpful to clinicians.

Despite numerous experimental and clinical studies on the EDPVR, there is relatively little theoretical knowledge, especially on the formulation of the corresponding curves. One commonly used method is to fit the EDPVR to an exponential form (Artrip et al., 2001; Burkhoff et al., 2005; Rodriguez et al., 2015; Shimizu et al., 2018),

$$P_{ED} = A\left(e^{B(V_{ED}-V_0)} - 1\right), \tag{1}$$

where P_{ED} is the end-diastolic pressure (EDP); V_{ED} is the end-diastolic volume (EDV); A and B are fitting parameters; V_0 is the reference volume when the ventricular pressure of the LV is zero. The exponential term in Eq. 1 is to reflect the exponential stress-strain relationship of the myocardial mechanical property. Its nonlinearity reflects the fact that diastolic stiffness steadily increases with loading (Ten Brinke et al., 2010).

Klotz et al. (2007) suggested that the EDPVR can be non-dimensionalized so that all values for different species, being dog, rat, or human, fall closely on a single curve, called the Klotz curve,

$$P_{ED} = A_n V_n^{B_n}, \text{ with } V_n = \frac{V - V_0}{V_{30} - V_0}, \tag{2}$$

where A_n and B_n are fitting parameters; V_n is the normalized volume; V_0 and V_{30} are the ventricular volumes when the ventricular pressures are 0 mmHg and 30 mmHg, respectively. The Klotz curve serves as a reference in some cardiovascular studies. In Nordsletten et al.'s study on human left ventricular diastolic and systolic function (Nordsletten et al., 2011), the Klotz curve served as a reference to validate the numerical data. Hadjicharalambous et al. (2015) took the Klotz curve as a matching target when evaluating the initial parameter set for 3D tagged MRI. Although widely used, the Klotz curve is an *ad hoc* empirical function describing the EDPVR, and does not have physical justification. Furthermore, it shows poor agreement with the experimental data and simulation data at small volumes (Klotz et al., 2007; Dabiri et al., 2018).

Besides the exponential model and the Klotz curve, other forms of fitting of the EDPVR can be found in the literature (Burkhoff et al., 2005). These fittings of different orders are more mathematical in nature and do not have sufficient physical implications. Thus, a deeper understanding of the EDPVR and its interaction with myocardial properties and cardiac disease warrants a physical model derived directly from the fundamentals of cardiac mechanics.

Although the EDPVR and ESPVR share common mechanisms, they have mostly been studied separately. Very idealized the ESPVR is assumed to be linear and can be fitted with $P_{ES} = E_{ES}(V_{ES} - V_0)$ (Sagawa, 1978; Burkhoff et al., 2005; Rodriguez et al., 2015; Shimizu et al., 2018). Therein P_{ES} and V_{ES} are the pressure and volume at the ES state, respectively; E_{ES} is the slope of the curve, thus the ES elastance. In reality, however, with different contractility, the ESPVR is nonlinear especially over a large volume range (Burkhoff et al., 1987; Burkhoff et al., 2005; Moriz et al., 2021). Some other fitting functions, such as the bilinear form Moriz et al.

(2021) and parabolic form Burkhoff et al. (1987) can also be found in the literature. Nakano et al. (1990) investigated the nonlinearity of the ESPVR and proposed a contractile index independent of ventricular size. In their work, the LV was mimicked by a thick-walled ellipsoid and the contractile index was used to calculate the wall stress based on the concept of mechanical work. P_{ES} and V_{ES} can then be connected with the relationship between wall stress and thickness. Experiments with 25 healthy dogs showed that the proposed contractile index was independent of ventricular size and geometry. Sato et al. (1998) measured the ESPVR of rat LV *in situ* with a catheter and observed contractility dependent nonlinearity in the ESPVR. Moriz et al. (2021) focused on the nonlinearity of the ESPVR and investigated the effect of different loading alterations on the shape of the ESPVR in pig hearts. The bilinear behavior of the ESPVR in their experimental data strengthens the argument that the linear model is only a special case of nonlinear ESPVR, which is a strong support for the physics-based ESPVR model with similar nonlinearity that we will present. A recent review of invasive analysis for the PV relationships in the LV, including both the EDPVR and ESPVR, can be found in Bastos et al. (2020).

Here we present a physics-based model that characterises both the EDPVR and the ESPVR. The model uses parameters derived from the properties of the heart under consideration. The physical properties, such as myocardial stiffness, thickness, and contractility, replace the extensive use of otherwise conjectured fitting parameters found in previous works, as discussed above. Section 2 presents the physics-based model. Section 3 offers a discussion of the model, including its validation and its predictions. Section 4 considers the implications and limitations of the model. Finally, a conclusion is given in Section 5.

2 The physics-based model

2.1 Model definition and theory

The schematic of our physics-based model in the reference state is shown in the left panel of Figure 2. The right panel shows an example of deformation with end-diastolic ventricular wall thinning. Conversely, the wall thickens during systolic contraction. Matching the simplicity of the single curve for either EDPVR or ESPVR, the cardiac shape is approximated by a thick-walled sphere. The use of such simplified geometries dates back to the early days of cardiac modeling and can be found still in modern research (Anani and Rahimi, 2016; Kalhöfer-Köchling, 2020). The reference geometry Ω_0 of the LV is shown on the left-hand side, whereas the right-hand side depicts the geometry in a deformed state. The inner and outer radius of the sphere for the reference geometry are R_{endo} and R_{epi}, respectively. The wall thickness is thus $R_{epi} - R_{endo}$. While in the deformed geometry, the inner and outer radius become r_{endo} and r_{epi}, correspondingly.

A spherical coordinate system is adopted so that its origin is located at the center of the sphere. The three orthogonal basis vectors of coordinate systems are $(\mathbf{e}_r,\mathbf{e}_\theta,\mathbf{e}_\varphi)$. A deformation maps a point $\mathbf{X}$ in the reference geometry Ω_0 to point $\mathbf{x}$ in the deformed geometry Ω. For a given point $\mathbf{X}$ in the reference geometry, the radial coordinate is R, while the corresponding radial coordinate of the point $\mathbf{x}$ in the deformed geometry is r. The second and third coordinates of the point, θ and φ, keep unchanged under deformation due to the assumption of centrosymmetry, which will be clarified later. The deformation gradient tensor is defined as

$$\mathbf{F} = \frac{\partial \mathbf{x}}{\partial \mathbf{X}}. \tag{3}$$

Under the spherical coordinate system, it is straightforward to get

$$\mathbf{F} = \mathrm{diag}\left(\lambda_\rho, \lambda_\theta, \lambda_\varphi\right), \tag{4}$$

where λ_ρ is the radial strain; λ_θ and λ_φ are two tangential strains.

We assume that the myocardium is incompressible, resulting in the volumetric strain $J = det(\mathbf{F}) = 1$, yielding the relation

$$\lambda_\rho \lambda_\theta \lambda_\varphi = 1. \tag{5}$$

The sphere only has expansion and contraction deformations, which means that the points in the domain only have radial displacement. We have the symmetry constraint

$$\lambda_\theta = \lambda_\varphi. \tag{6}$$

The strain λ_θ can be calculated by the ratio of the perimeter l of the cross-section through the spherical center (which is represented by the red dotted circle in Figure 2) on the deformed geometry and L on the reference geometry $\lambda_\theta = l/L$, yielding

$$\lambda_\theta = \frac{r}{R}. \tag{7}$$

Substituting Eqs 6, 7 into Eq. 5, we can get the radial strain

$$\lambda_\rho = \frac{R^2}{r^2}. \tag{8}$$

Numerically, the right Cauchy-Green strain tensor $\mathbf{C}$ is a better choice for solving the balance equation than the deformation gradient tensor $\mathbf{F}$, since the former is symmetric and positive definite for all points $\mathbf{X} \in \Omega_0$, which reduces computational costs. Said right Cauchy-Green strain tensor is defined as

$$\mathbf{C} = \mathbf{F}^T\mathbf{F}. \tag{9}$$

Substituting Eqs 4–6 into Eq. 9, the right Cauchy-Green deformation tensor reads

$$\mathbf{C} = \mathrm{diag}\left(\lambda_\rho^2, \frac{1}{\lambda_\rho}, \frac{1}{\lambda_\rho}\right). \tag{10}$$

The first invariant of the right Cauchy-Green deformation tensor I_1 can be expressed as

$$I_1 = \lambda_\rho^2 + \frac{2}{\lambda_\rho}. \tag{11}$$

Due to the incompressibility of the myocardium, the volume between the inner surface and the red dotted spherical surface (see Figure 2 for reference), stays constant. It follows straightforward that

$$R^3 - R_{\mathrm{endo}}^3 = r^3 - r_{\mathrm{endo}}^3. \tag{12}$$

The geometrical parameters are further normalized by the inner radius R_{endo} and the ventricular volume V_0 of the reference geometry as follows

$$\widehat{R} = \frac{R}{R_{\mathrm{endo}}}, \hat{r} = \frac{r}{R_{\mathrm{endo}}}, \delta = \frac{R - R_{\mathrm{endo}}}{R_{\mathrm{endo}}}, \Delta = \frac{R_{\mathrm{epi}} - R_{\mathrm{endo}}}{R_{\mathrm{endo}}}, \widehat{V} = \frac{V}{V_0}, \tag{13}$$

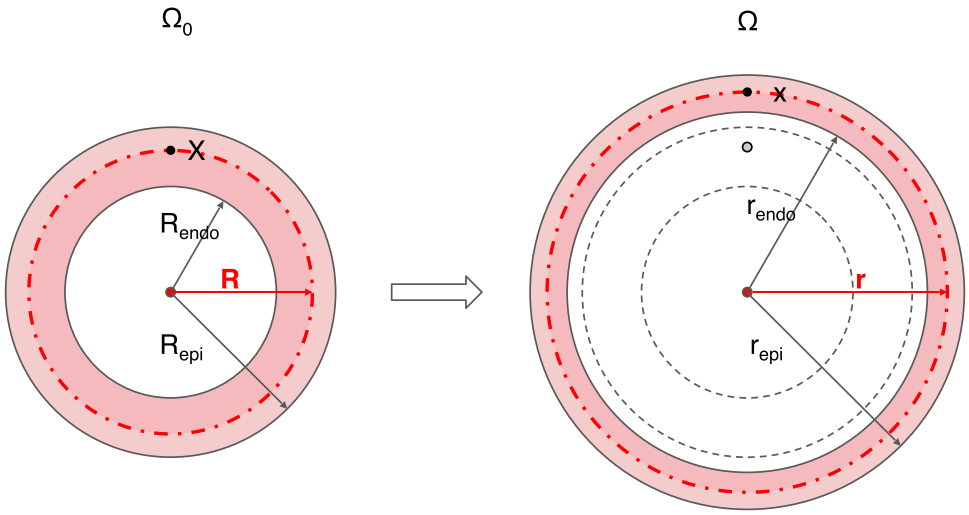

FIGURE 2
Schematic diagram of the geometry and its deformation in the physics-based model. A thick-walled sphere is used to mimic the LV, whose cross section through the sphere center is shown. The reference geometry Ω_0 with inner radius R_{endo} and outer radius R_{epi} is given on the left side. The deformed geometry Ω in the diastolic state with inner radius r_{endo} and outer radius r_{epi} is shown on the right. For any point **X** in the reference geometry Ω_0, the corresponding position on the deformed geometry Ω is **x**, with radial coordinate R and r, respectively. Centrosymmetric deformation is assumed for the model. Endo, endocardium; epi, epicardium.

where Δ is the normalized thickness; V is the ventricular volume at deformed geometry. With Eqs 12, 13, the normalized radius can be expressed as

$$\hat{r} = \left(\hat{R}^3 + \hat{V} - 1\right)^{1/3}. \tag{14}$$

The total elastic energy W stored in the myocardium can be calculated by integrating the energy density function Ψ over the domain Ω_0

$$W = \int_{\Omega_0} \Psi \mathrm{d}\Omega. \tag{15}$$

The sphere experiences an inner pressure P, representing the blood pressure inside the LV. While the outer pressure is set to zero, indicating a free boundary condition. Based on classical mechanics, it is known that any mechanical work W performed on the sphere due to a given internal pressure P follows the relation

$$P = \frac{\mathrm{d}W}{\mathrm{d}V}. \tag{16}$$

Substituting Eqs 9–15 into Eq. 16, we get an important relationship

$$P = -2\int_0^{\Delta} \frac{\lambda_\rho^2}{\hat{r}} \frac{\mathrm{d}\Psi}{\mathrm{d}\lambda_\rho} \mathrm{d}\delta. \tag{17}$$

Therein, the ventricular pressure is expressed as the integral of the energy density function Ψ over the domain defined by the normalized thickness. The EDPVR and ESPVR can be further deducted based on this relationship. Besides such mechanical work approach, another approach based on stress analysis can also be found in Kalhöfer-Köchling (2020).

2.2 End-diastolic pressure-volume relationship

The myocardium is considered to be a homogeneous, incompressible, anisotropic, and fiber-reinforced soft material that generates active forces. Inspired by experimental data, several constitutive laws (energy density function Ψ) for the myocardium have been developed in the last decades, including the orthotropic Holzapfel-Ogden model (Holzapfel and Ogden, 2020) and our recently developed squared generalized structure-tensor (SGST) models (Kalhöfer-Köchling et al., 2020), in which the fiber dispersion of the myocardium is taken into account. Considering the microstructure of the myocardium, these constitutive laws contain different contributions of isotropic, fibrous, and laminar structures as well as their coupling, and are used for simulations at tissue or organ level (Baillargeon et al., 2014; Chabiniok et al., 2016; Kalhöfer-Köchling, 2020).

As a first approximation, by neglecting the anisotropy of the cardiac tissue, the isotropic energy function is considered in this work

$$\Psi = \frac{a}{2b}\left(e^{b(I_1-3)} - 1\right), \tag{18}$$

where a and b are mechanical parameters representing the material property, i.e., the stiffness, which can be obtained from experiments.

Incorporating the constitutive law Eq. 18 into Eq. 17, one gets the passive contribution of the myocardium on the ventricular pressure, implying the EDPVR

$$P_{ED} = 2a\int_0^{\Delta} \frac{1-\lambda_\rho^3}{\hat{r}} e^{b(I_1-3)} \mathrm{d}\delta. \tag{19}$$

Therein, the input parameters are a, b and Δ, while the output is a function indicating the relation between the ventricular volume and the ventricular pressure at the ED state.

2.3 End-systolic pressure-volume relationship

There are two contributions to the stresses and strains in cardiac muscle tissue: the passive and the active components. As for the passive contribution, the tissue generates resistive stress when it is deformed. This tension contributes to the ventricular pressure of the LV. On the other hand, the tissue actively contracts and the active force generated inside the tissue also contributes to the ventricular pressure. Active contraction of the cardiac muscle can be modelled in two different ways: using the additive stress approach or the multiplicative strain approach, as described in Pezzuto (2013). We have adopted the former due to its simplicity and intuitive nature. Thus, we have the total pressure $P = P_p + P_a$ and the energy function $\Psi = \Psi_p + \Psi_a$. The indices p and a represent the passive and active parts, respectively.

To model the ESPVR, an active contribution, which indicates the active force generated by the myocardium during the ES state, is added onto the passive contribution Eq. 18. Such an active contribution reads

$$\Psi_a = T_a\left(\frac{\lambda^2}{2} - \lambda_0\lambda\right), \tag{20}$$

where T_a is the maximum active stress; $\lambda_0 = l_0/l_r$ with the sarcomere smallest length $l_0 = 1.58\ \mu$m and rest length $l_r = 1.85\ \mu$m (Guccione et al., 2001). The strain of the sarcomere λ is defined as

$$\lambda = \sqrt{\mathbf{C}:\mathbf{H_a}}. \tag{21}$$

The active force structure tensor $\mathbf{H_a}$ is defined such that contractile forces act in the tangential plane of the myocardium

$$\mathbf{H_a} = \mathbf{I} - \mathbf{e_r} \otimes \mathbf{e_r}, \tag{22}$$

Substituting Eqs 21, 22 into Eq. 20, the energy function for active force reads

$$\Psi_a = T_a\left(\frac{1}{\lambda_\rho} - \lambda_0\sqrt{\frac{2}{\lambda_\rho}}\right). \tag{23}$$

Incorporating Eq. 23 into Eq. 17, we obtain the active contribution of pressure

$$P_a = 2T_a\int_0^\Delta \frac{1 - \lambda_0\sqrt{\frac{\lambda_\rho}{2}}}{\hat{r}}\,\mathrm{d}\delta. \tag{24}$$

The pressure at the ES state contains both the passive and active parts. Adding Eq. 24 onto Eq. 19, we get the ESPVR

$$P_{ES} = 2\int_0^\Delta \frac{a\left(1-\lambda_\rho^3\right)e^{b(I_1-3)} + T_a\left(1-\lambda_0\sqrt{\lambda_\rho/2}\right)}{\hat{r}}\,\mathrm{d}\delta. \tag{25}$$

3 Validation and discussion

3.1 Physics-based model: EDPVR

To validate the physics-based EDPVR model, we fit different models to the dataset from Klotz et al. (2006) and Klotz et al. (2007) and compare them in Figure 3. The dataset contains *ex vivo* EDPVR data for 80 human hearts. The fitting was implemented by minimizing the mean squared error (MSE) for the models. The full dataset with pressure up to 30 mmHg, and a subset with a physiologically reasonable pressure range (up to 20 mmHg), were considered respectively.

As we can see in Figures 3A, B, the green solid lines representing the physics-based model show a good fit to the experimental data. We compared our model with two other widely used EDPVR models, i.e., the exponential model (Artrip et al., 2001; Rodriguez et al., 2015; Shimizu et al., 2018) and the Klotz curve (Klotz et al., 2007). The Klotz curve (Eq. 2) belongs to the family of polynomial power functions, while the former (Eq. 1) is classified in the form of exponential functions. Our physics-based model entails the combination of an exponential energy function (Eq. 18) with a volume integral, hence resulting in exponential behaviour. It should be noted that during the curve fitting the original exponential model was adapted to the same normalized form as the Klotz curve. This was done by replacing the term $V - V_0$ with V_n, which yields $P_{ED} = A(e^{BV_n} - 1)$.

The optimized parameters for the three models are given in Table 1. Contrary to previous models, the parameters in our model have a physical meaning. For example, a and b together reflect the stiffness of the material. The fitted values of a and b of our model are close to most values from experiments and simulations in the literature (Baillargeon et al., 2014; Nikou et al., 2016), although parameter estimates themselves often vary considerably across different datasets and experimental protocols. These two parameters are exactly the same as those in the isotropic constitutive law (Eq. 18). Δ is the normalized thickness of the LV wall, which is an important measure of the ventricular geometry.

The resulting curves of the three models in the full dataset are shown in Figure 3A. The MSEs of the original exponential model, the Klotz curve, and the physics-based model are 2.82, 3.19, and 3.08, respectively. Since our physics-based model uses an exponential constitutive law, it is fundamentally similar to the original exponential model. This is why the curves of the physics-based model and the original exponential model are almost identical, and both perform better than the Klotz curve. Figure 3C presents the residuals of the exponential model and the Klotz curve, using the physics-based model as a reference. It can be seen that the exponential model is much closer to the physics-based model, especially in the region with small volumes. It is also worth mentioning that the Klotz curve is not consistent with its definition at the maximum volume or pressure. When the normalized volume V_n is equal to 1, the resulting pressure in the Klotz curve is the same as the value of A_n, which, by design, may be different from the expected 30 mmHg.

The physics-based model shows its strong utility for small volumes. The normalized volume V_n of this region ranges from 0 to 0.8, corresponding to the pressure 0–20 mmHg, which covers the EDP of the human heart. To better evaluate these three models within this physiologically reasonable range, we generated a sub-dataset with pressures no more than 20 mmHg. The results are shown in Figures 3B, D. Here, the physics-based model shows the best fit with a MSE of 2.46. The MSE for the exponential model is 2.48. The Klotz curve has the worst fit

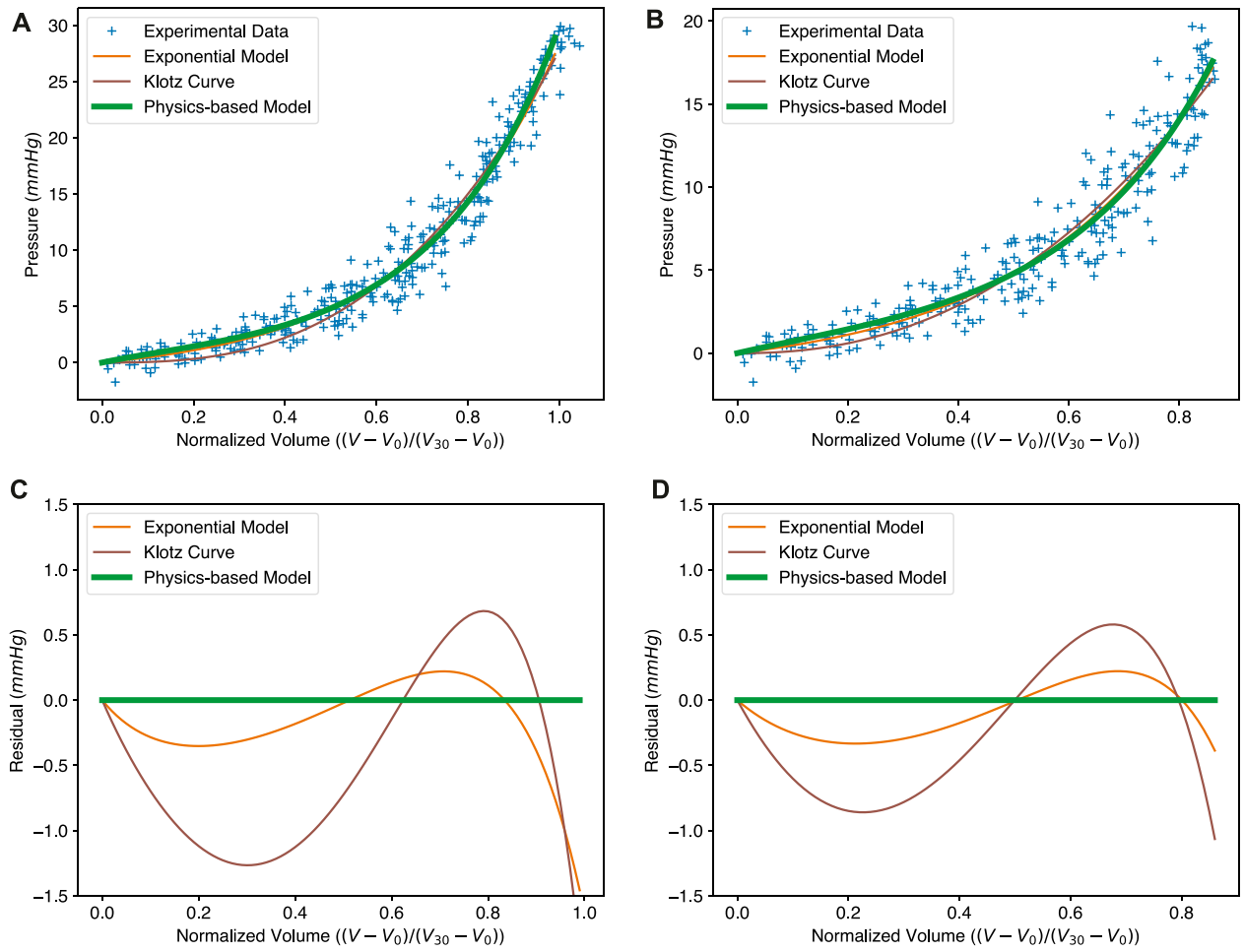

FIGURE 3
Comparison between the exponential model (Eq. 1), the Klotz curve (Eq. 2) and the physics-based model (Eq. 19) for the EDPVR. **(A–C)** The fitted curves to the full experimental dataset and the corresponding residuals. MSEs: exponential model, 2.82; Klotz curve, 3.19; physics-based model, 3.08. **(B–D)** The fitted curves to the sub-dataset and the corresponding residuals, with pressure no more than 20 mmHg. MSEs: exponential model, 2.48; Klotz curve, 2.69; physics-based model, 2.46. Model parameters for subfigures **(A–C)** and **(B–D)** are listed in Table 1.

TABLE 1 The least-square fits for the three EDPVR models with respect to the datasets presented in Figure 3. MSE, Mean Squared Error.

	Exponential model, Eq. 1			Klotz curve, Eq. 2			Physics-based model, Eq. 19			
	A (kPa)	B	MSE	A_n (kPa)	B_n	MSE	Δ	a (kPa)	b	MSE
Full dataset	0.16	3.18	2.82	3.70	2.76	3.19	0.27	1.15	3.82	3.08
Sub dataset	0.18	3.07	2.48	3.10	2.27	2.69	0.27	2.10	8.71	2.46

with a MSE of 2.69, indicating its weakness at small ventricular volumes.

The Klotz curve is often used as a reference when estimating material parameters of myocardium, like stiffness, in numerical simulations (Krishnamurthy et al., 2013b; Hadjicharalambous et al., 2017; Sack et al., 2018). These simulations mostly use exponential constitutive laws to describe the mechanical properties of the myocardium. Based on the above-mentioned comparison, the new physics-based model shows the capacity to replace the Klotz curve in similar simulations in the future.

Because of its bottom-up, physical nature, the model can be used to predict the EDPVR of a ventricle with given information, such as mechanical properties and thickness of the myocardium. In Figure 4A, Dokos et al. (2002) represents the parameters for pig hearts, Demiray (1972) and Marx et al. (2022) are for the human hearts. We further performed finite element simulations using COMSOL Multiphysics (version 6.0.0.405) with the same parameter sets. The geometry of the finite element model is the same as that of the physical model, i.e., a thick-walled sphere. The normalized inner radius and thickness are 1.0 and

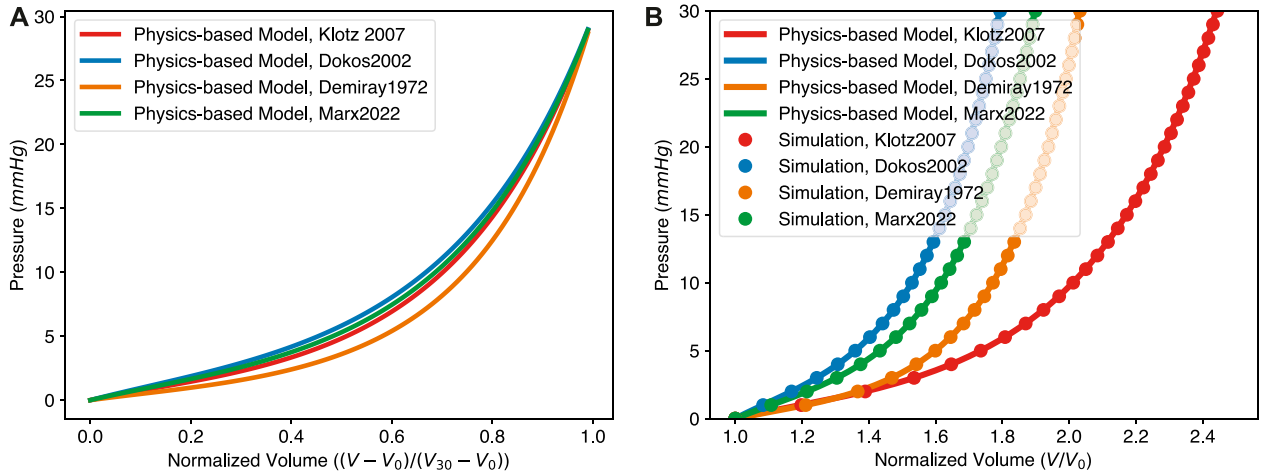

FIGURE 4
The physics-based model predicts the effect of varying mechanical properties on the EDPVR with *in silico* validation. **(A)** The EDPVR curves predicted by the physics-based model with different parameter sets. **(B)** In silico validation of the physics-based model. Simulation results agree with the physics-based model very well for each set of parameters. Parameters used in the physics-based model: Klotz 2007: $a = 1.15$ kPa, $b = 3.82$; Dokos 2002: $a = 2.52$ kPa, $b = 6.79$; Demiray 1972: $a = 1.00$ kPa, $b = 6.5$; Marx 2022: $a = 1.98$ kPa, $b = 6.19$. For all curves: $\Delta = 0.27$.

0.27, respectively. The inner surface was subjected to a constant pressure mimicking the ventricular pressure from blood, while the outer surface was free. Due to rotational symmetry, only 1/8 of the sphere with 26,392 tetrahedral elements (119,614 degrees of freedom) was simulated using the symmetry boundary condition. Equation 18 was used for the passive myocardium. The volumetric energy function $\Psi_v = \kappa((J^2-1)/2 - \ln J)$ was applied to ensure tissue incompressability. The bulk modulus κ was 1 GPa; $J = \det(\mathbf{F})$ was the volumetric strain. Finally, in Figure 4B the normalized volume V/V_0 and pressure obtained from the simulation are compared with the algebraic solutions of our physics-based EDPVR model. The perfect match between the finite element simulation and the theoretical model is not surprising as they are conceptually identical and only the calculation scheme differs. This is a demonstration of the relation between constitutive models commonly employed in cardiac mechanics simulations and our algebraic equation.

By changing the thickness Δ in our model, we studied how myocardium thickness affects the EDPVR of the LV, as shown in Figure 5A. An increased myocardium thickness leads to an upward lift of the EDPVR curve. To keep the same volume, higher pressure is needed when increasing the thickness of the LV, as shown in Figure 5B. This reflects the strong utility of a physics-based model over that of simply fit, i.e., the physics-based model is predictive over a wide range of parameters while a fit cannot.

3.2 Physics-based model: ESPVR

The ESPVR describes the relationship between ventricular pressure and volume at the ES state of the LV as loading conditions change. It is composed of two parts, as shown in Eq. 25. The first part is identical to the EDPVR and the second part comes from the active force generated by the myocardium. The two contributions are shown in Figure 6A. Therein, the solid blue line is the overall ESPVR, while the dashed green one is from the active contraction. A large proportion of the pressure in the LV during the contraction is due to the active force generated by the myocardium. The shape of the ESPVR, especially when the normalized ESV is less than 1.0, is mainly determined by the passive resistance due to the deformation of the myocardium. In addition, the ESPVR with small volume is roughly linear, while the overall curve is almost bilinear. This implies that both the linear or bilinear forms of the ESPVR used in the literature have some validity. Please also notice that for the passive part of the ESPVR, the pressure is shown as a negative value. Negative pressure means that the tissue is resisting the deformation caused by its own active contraction. The greater the deformation at ES state, the more negative pressure (resistance stress) is generated, so that the required ventricular pressure is lower. It should be noted that the resistance stress increases in a nonlinear fashion with the decrease of the ESV, due to the nonlinear stress/strain behavior of the tissue. This results in the nonlinear shape of the ESPVR. Our model also shows that the positive slope of the ESPVR is mainly due to the decrease of the resistance stress as ESV increases.

To validate the proposed ESPVR model, we performed an additional finite element simulation, with the same geometry, mesh, boundary condition and volumetric energy function as previously considered for Figure 4B. The active force generated by the myocardium was determined by the energy function Eq. 20. For the passive response of the myocardium, the energy function was chosen according to Eq. 18. Parameters used in both the physics-based ESPVR model and numerical simulation are $a = 1.15$ kPa, $b = 3.82$, and $T_a = 76.90$ kPa. In Figure 6B, the orange dots present simulation results while the blue solid line is from the physics-based ESPVR model. In a large region of the normalized volume, the ESPVR predicted by the physics-based model agrees with the simulation results very well.

To further check the validity of our physics-based ESPVR model, we compared it with experimental ESPVR data. The experimental

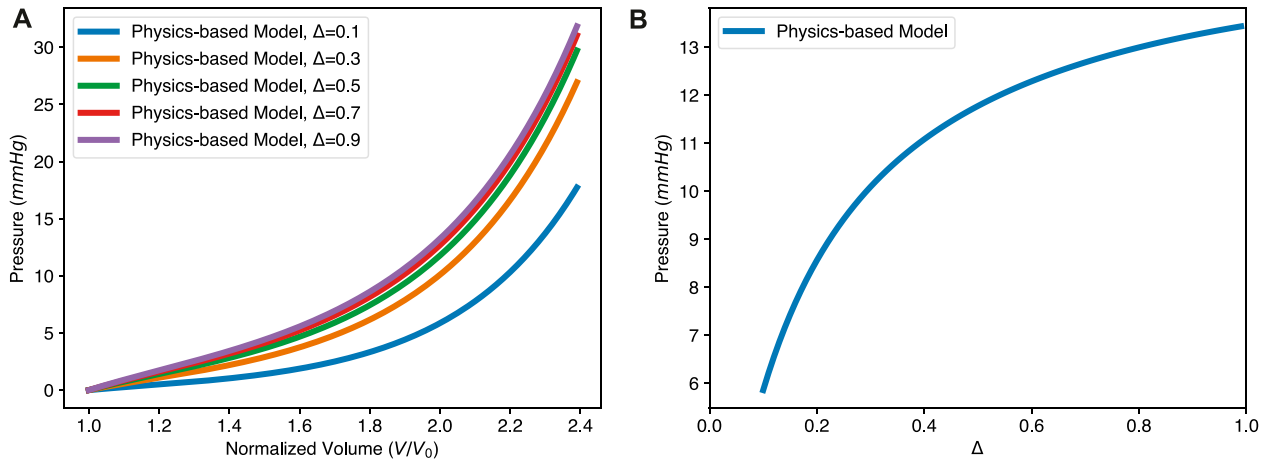

FIGURE 5
The physics-based model predicts the effect of varying myocardial thickness on the EDPVR. **(A)** The EDPVR curve moves upward with the increase of thickness Δ, while *a* and *b* remain constant. **(B)** Nonlinear relationship between the ventricular pressure and the thickness, with constant normalized volume $V/V_0 = 2.0$. Parameters used in the physics-based model: $a = 1.15$ kPa and $b = 3.82$.

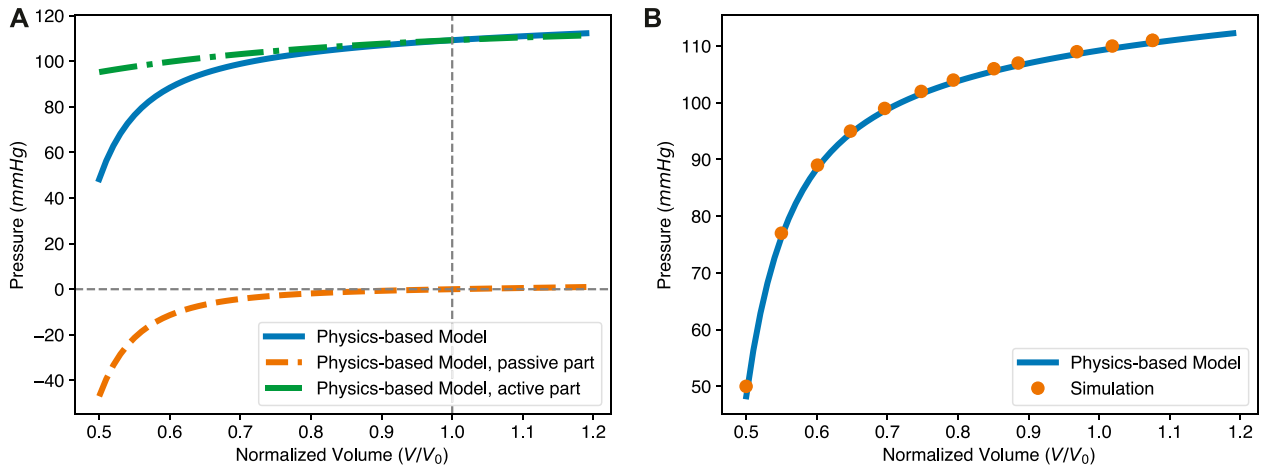

FIGURE 6
The intrinsic structure and *in silico* validation of the physics-based ESPVR model. **(A)** The pressure in the ESPVR has two contributions, one from the active contraction and the other one from the passive resistance of the tissue. The overall level of pressure is mainly determined by the active stress. The shape, especially at the lower ventricular volume region from 0.5 to 0.7, is mostly influenced by passive resistance. **(B)** The theoretical ESPVR curve fits very well with the simulation results. The parameters for both the theoretical and simulation are $\Delta = 0.27$, $a = 1.15$ kPa, $b = 3.82$, and $T_a = 76.9$ kPa.

data for a pig heart was extracted from Moriz et al. (2021), by changing afterload pressure. The stress-free volume of the LV, V_0, was assumed to be 50 mL based on Figure 3B of Moriz et al. (2021). Since the mechanical property and contractility of that pig heart were unknown, $a = 2.52$ kPa and $b = 6.79$ (Dokos 2002 in Figure 4) were adopted from Dokos et al. (2002), which performed shear test for cardiac tissue of the same specie; $T_a = 81.89$ kPa was obtained by fitting our ESPVR model to the experimental points and this value is physiologically reasonable. Other parameters used in our physics-based ESPVR model are $\Delta = 0.27$ and $\lambda_0 = 0.85$ as usual. As shown in Figure 7, our model shows good agreement with the experimental data with a maximum relative error of 6.77%.

4 Implications and limitations

Adjusting the parameters of the physics-based model allows the study of left ventricular diseases, such as left ventricular hypertrophy, decreased contractility, and diastolic heart failure. For example, for patients with hypertrophic cardiomyopathy, the heart wall thickens to maintain pump function. This effect is easily visualized with

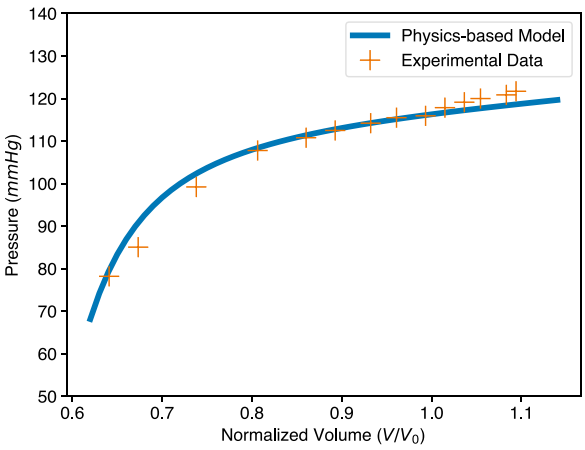

FIGURE 7
Comparison of the physics-based model and experimental data for the ESPVR. The physics-based ESPVR model is shown in blue. The experimental data of a pig heart, shown as orange crosses, is from Moriz et al. (2021). The volume of the original data is normalized, assuming stress-free volume V_0 = 50 mL. Parameters used in the physics-based model: Δ = 0.27, a = 2.52 kPa, b = 6.79, and T_a= 81.89 kPa.

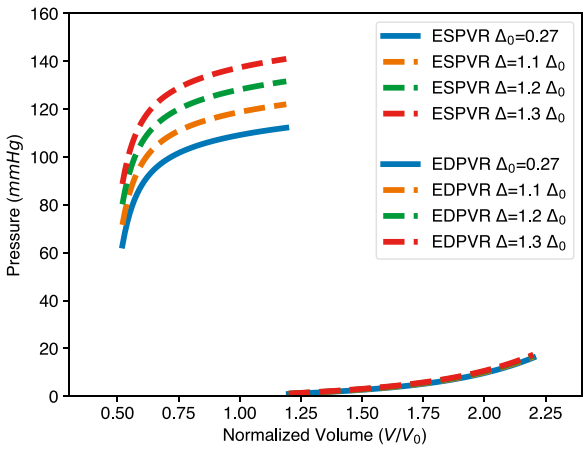

FIGURE 8
Effect of wall thickness on the EDPVR and ESPVR predicted by the physics-based model. Δ_0 = 0.27 is the LV wall thickness of a healthy human heart and is therefore considered here as a reference case. The change in wall thickness has a significant effect on the ESPVR, but a relatively small effect on the EDPVR. Parameters used in the physics-based model: a =1.15 kPa, b =3.82, and T_a =76.9 kPa.

our physics-based model (see Figure 5). In addition, the passive parameters a and b can be manipulated to better understand such disease.

With the physics-based model, one can generate both the EDPVR and ESPVR for the same LV in the same plot, as shown in Figure 8. With given information such as pressure or volume in the ED and ES states, the PV loop will be determined. Therefore, indicators of pump function, such as the stroke volume (SV) and ejection fraction (SV/EDV) can also be calculated. Furthermore, considering new therapies for heart failure, such as engineered muscle tissue (Zimmermann et al., 2006; Tiburcy et al., 2017), Figure 8 also shows that increasing wall thickness by implanting contractile tissue patch will increase the pump function of the LV. This is because when the wall thickness is increased, the EDPVR hardly changes, while the ESPVR is lifted to the upper left.

Our physics-based model provides even more latitude by combining pressure, volume, shape, active force, and mechanical properties of the LV into a unified framework. We notice that 3D printed artificial hearts (Lee et al., 2019; Noor et al., 2019) or ventricles (Kolawole et al., 2021) are attracting increased attention recently, bringing new opportunities for the treatment of heart diseases. The physics-based model proposed in this work can be used to guide 3D printing. For example, with certain mechanical properties and the targeted pump function, our model can predict the required thickness of the heart chamber. For a given ventricular pressure P for which the artificial heart is designed to experience, there is a threshold that the active force T_a must exceed, which can also be obtained from our model.

Furthermore, considering the dynamic cardiac cycle, the ratio of active force T_a to ventricular pressure P gradually increases from diastole to systole. When this ratio exceeds a certain threshold, the LV starts to contract, which means that the volume of the LV is smaller than the stress-free volume V_0. This stress-free or pressure-free geometry is widely used in heart simulations. Our model shows that this threshold is only related to the LV thickness and with this value one can obtain the stress-free volume and the associated reference time.

The sensitivity of the predicted result to the input parameters of the model was also examined. Sensitivity analysis quantifies the relationship between the uncertainty of the model output and the uncertainty of the input parameters (Saltelli et al., 2004). A physiologically reasonable base set of parameters (a = 1.15 kPa, b = 3.82, Δ = 0.27, T_a = 76.9 kPa, V/V_0 = 1.5 for EDPVR and 0.8 for ESPVR) was considered. The same parameter set was also used in Figure 8. We first performed the one-at-a-time sensitivity analysis, i.e., we varied each input parameter (a, b, Δ and T_a) by 1{%}, 5{%}, 10{%} and 20{%} while keeping the others unchanged, and examined the resulting output (P) change. This is assessed quantitatively in terms of the ratio S between the relative change in the output and the relative change in an input parameter. According to Eqs 19, 25, it can be found that P is linearly related to a and T_a, while the absolute values of S respect to b and Δ are less than 1. The results indicate that the behaviour of the proposed model is stable around the base set. We further calculated the Hessian matrix of our model and found that Δ is weakly coupled with other input parameters. Therefore, we recommend that only mechanical properties (a, and b) and contractility (T_a) be considered when fitting experimental data using this model.

Last but not least, by reducing b to zero, the model reduces to a rubber spherical shell of Neo-Hookean's material. The elastic instabilities (Anssari-Benam et al., 2022) of spherical inflation can also be reproduced with our model, revealing possible applications of our model beyond the heart.

We are aware that our reductionistic approach cannot fully describe cardiac mechanics. Yet, this simplicity makes it a powerful

tool to support comprehensive simulations and diagnostics. The ventricular geometry is not perfectly spherical and, whereas the myocardium is layered and fiber-reinforced soft matter with rotated and dispersed fibers (Sommer et al., 2015; Nielles-Vallespin et al., 2017; Kalhöfer-Köchling et al., 2020; Khalique et al., 2020; Reichardt et al., 2020). If all these factors are to be considered, the complexity of the model increases significantly. For such a complex situation, it is recommended to use numerical simulations rather than theoretical models. If the overall pump function and the pressure-volume relationship of the left ventricle are to be considered only, the current simplifications are believed sufficient.

An easy-to-use Python code, for both the physics-based EDPVR and ESPVR, is provided. Please check Data availability statement for more details.

5 Conclusion

To conclude, we proposed a bottom-up physics-based model incorporating the EDPVR and ESPVR of the LV. The two contributions in this model show the sources of pressure in the end-diastolic and end-systolic states. The model fits existing experimental data well and shows good agreement with simulation results. The model has been shown to be suitable for evaluating LV stiffness and contractility. Conversely, the model can predict the EDPVR and ESPVR of the LV based on the parametric and geometric information of the myocardium. It can also be used to study the relationship between the mechanical properties of the LV and its pump function. The proposed model might provide insight into the study of cardiac mechanisms and be used in clinical medicine.

Data availability statement

A code of the physics-based model is publicly available at https://github.com/Kinsmo/PBPVR. Alternatively, a web application based on the code can also be found at https://physical-pvr.streamlit.app/. The original contributions presented in the study are included in the article/Supplementary Material, further inquiries can be directed to the corresponding author.

Author contributions

YZ and MK-K contributed equally. MK-K proposed the model for the EDPVR. YZ proposed the model for the ESPVR. YZ, MK-K, and YW performed data analysis, and drafted the manuscript. YZ, MK-K, EB, and YW reviewed the manuscript. All authors contributed to the article and approved the submitted version.

Funding

This work was supported by the Max Planck Society and the German Center for Cardiovascular Research.

Acknowledgments

We thank Wolfram Zimmermann and Tim Meyer for their continuous support and inspiring scientific discussions.

Conflict of interest

The authors declare that the research was conducted in the absence of any commercial or financial relationships that could be construed as a potential conflict of interest.

Publisher's note

References

Anani, Y., and Rahimi, G. (2016). Stress analysis of thick spherical pressure vessel composed of transversely isotropic functionally graded incompressible hyperelastic materials. *Lat. Am. J. Solids Struct.* 13 (3), 407–434. doi:10.1590/1679-78252386

Anssari-Benam, A., Bucchi, A., and Saccomandi, G. (2022). Modelling the inflation and elastic instabilities of rubber-like spherical and cylindrical shells using a new generalised neo-hookean strain energy function. *J. Elast.* 151 (1), 15–45. doi:10.1007/s10659-021-09823-x

Artrip, J. H., Oz, M. C., and Burkhoff, D. (2001). Left ventricular volume reduction surgery for heart failure: a physiologic perspective. *J. Thorac. Cardiovasc. Surg.* 122 (4), 775–782. doi:10.1067/mtc.2001.116208

Baillargeon, B., Rebelo, N., Fox, D. D., Taylor, R. L., and Kuhl, E. (2014). The living heart project: a robust and integrative simulator for human heart function. *Eur. J. Mech. A/Solids* 48 (1), 38–47. doi:10.1016/j.euromechsol.2014.04.001

Bastos, M. B., Burkhoff, D., Maly, J., Daemen, J., den Uil, C. A., Ameloot, K., et al. (2020). Invasive left ventricle pressure-volume analysis: overview and practical clinical implications. *Eur. Heart J.* 41 (12), 1286–1297. doi:10.1093/eurheartj/ehz552

Burkhoff, D., Mirsky, I., and Suga, H. (2005). Assessment of systolic and diastolic ventricular properties via pressure-volume analysis: a guide for clinical, translational, and basic researchers. *Am. J. Physiology - Heart Circulatory Physiology* 289 (2), H501–H512. doi:10.1152/ajpheart.00138.2005

Burkhoff, D., Sugiura, S., Yue, D. T., and Sagawa, K. (1987). Contractility-dependent curvilinearity of end-systolic pressure-volume relations. *Am. J. Physiology - Heart Circulatory Physiology* 252, H1218–H1227. doi:10.1152/ajpheart.1987.252.6.H1218

Chabiniok, R., Wang, V. Y., Hadjicharalambous, M., Asner, L., Lee, J., Sermesant, M., et al. (2016). Multiphysics and multiscale modelling, data–model fusion and integration of organ physiology in the clinic: ventricular cardiac mechanics. *Interface Focus* 6 (2), 20150083. doi:10.1098/rsfs.2015.0083

Dabiri, Y., Sack, K. L., Shaul, S., Sengupta, P. P., and Guccione, J. M. (2018). Relationship of transmural variations in myofiber contractility to left ventricular ejection fraction: implications for modeling heart failure phenotype with preserved ejection fraction. *Front. physiology* 9, 1003. doi:10.3389/fphys.2018.01003

Demiray, H. (1972). A note on the elasticity of soft biological tissues. *J. Biomechanics* 5 (3), 309–311. doi:10.1016/0021-9290(72)90047-4

Dokos, S., Smaill, B. H., Young, A. A., and LeGrice, I. J. (2002). Shear properties of passive ventricular myocardium. *Am. J. Physiology - Heart Circulatory Physiology* 283 (6), H2650–H2659. doi:10.1152/ajpheart.00111.2002

Gilbert, S. H., Benson, A. P., Pan, Li, and Holden, A. V. (2007). Regional localisation of left ventricular sheet structure: integration with current models of cardiac fibre, sheet and band structure. *Eur. J. Cardio-thoracic Surg.* 32 (2), 231–249. doi:10.1016/j.ejcts.2007.03.032

Goto, Y., Jin, Y., Saito, M., Haze, K., Sumiyoshi, T., Fukami, K., et al. (1985). Effects of right ventricular ischemia on left ventricular geometry and the end-diastolic pressure-volume relationship in the dog. *Circulation* 72 (5), 1104–1114. doi:10.1161/01.cir.72.5.1104

Guccione, J. M., Moonly, S. M., Moustakidis, P., Costa, K. D., Moulton, M. J., Ratcliffe, M. B., et al. (2001). Mechanism underlying mechanical dysfunction in the border zone of left ventricular aneurysm: a finite element model study. *Ann. Thorac. Surg.* 71 (2), 654–662. doi:10.1016/s0003-4975(00)02338-9

Hadjicharalambous, M., Asner, L., Chabiniok, R., Sammut, E., Wong, J., Peressutti, D., et al. (2017). Non-invasive model-based assessment of passive left-ventricular myocardial stiffness in healthy subjects and in patients with non-ischemic dilated cardiomyopathy. *Ann. Biomed. Eng.* 45 (3), 605–618. doi:10.1007/s10439-016-1721-4

Hadjicharalambous, M., Chabiniok, R., Asner, L., Sammut, E., Wong, J., Carr-White, G., et al. (2015). Analysis of passive cardiac constitutive laws for parameter estimation using 3D tagged MRI. *Biomechanics Model. Mechanobiol.* 14 (4), 807–828. doi:10.1007/s10237-014-0638-9

Holzapfel, G. A., and Ogden, R. W. (2020). Constitutive modelling of passive myocardium: a structurally based framework for material characterization. *Philosophical Trans. R. Soc. A Math. Phys. Eng. Sci.*, 367(1902), 3445–3475. doi:10.1098/rsta.2009.0091

Kalhöfer-Köchling, M., Bodenschatz, E., and Wang, Y. (2020). Structure tensors for dispersed fibers in soft materials. *Phys. Rev. Appl.* 13 (6), 064039. doi:10.1103/physrevapplied.13.064039

Kalhöfer-Köchling, M. (2020). *Constitutive modeling for tissue engineered heart repair*. Phd dissertation. Göttingen: University of Göttingen.

Khalique, Z., Ferreira, P. F., Scott, A. D., Nielles-Vallespin, S., Firmin, D. N., and Pennell, D. J. (2020). Diffusion tensor cardiovascular magnetic resonance imaging: a clinical perspective. *JACC Cardiovasc. Imaging* 13 (5), 1235–1255. doi:10.1016/j.jcmg.2019.07.016

Klotz, S., Dickstein, M. L., and Burkhoff, D. (2007). A computational method of prediction of the end-diastolic pressure-volume relationship by single beat. *Nat. Protoc.* 2 (9), 2152–2158. doi:10.1038/nprot.2007.270

Klotz, S., Hay, I., Dickstein, M. L., Yi, G-H., Wang, J., Maurer, M. S., et al. (2006). Single-beat estimation of end-diastolic pressure-volume relationship: a novel method with potential for noninvasive application. *Am. J. Physiology - Heart Circulatory Physiology* 291 (1), 403–412. doi:10.1152/ajpheart.01240.2005

Kolawole, F. O., Peirlinck, M., Cork, T. E., Wang, V. Y., Dual, S. A., Levenston, M. E., et al. (2021). "A framework for evaluating myocardial stiffness using 3D-printed heart phantoms," in *Functional imaging and modeling of the heart*. Editors D. B. Ennis, L. E. Perotti, and V. Y. Wang (Cham: Springer), 305–314. doi:10.1007/978-3-030-78710-3_30

Krishnamurthy, A., Villongco, C. T., Chuang, J., Frank, L. R., Nigam, V., Belezzuoli, E., et al. (2013a). Patient-specific models of cardiac biomechanics. *J. Comput. Phys.* 244 (4–21), 4–21. doi:10.1016/j.jcp.2012.09.015

Krishnamurthy, A., Villongco, C. T., Chuang, J., Frank, L. R., Nigam, V., Belezzuoli, E., et al. (2013b). Patient-specific models of cardiac biomechanics. *J. Comput. Phys.* 244, 4–21. doi:10.1016/j.jcp.2012.09.015

Lee, A., Hudson, A. R., Shiwarski, D. J., Tashman, J. W., Hinton, T. J., Yerneni, S., et al. (2019). 3D bioprinting of collagen to rebuild components of the human heart. *Science* 365 (6452), 482–487. doi:10.1126/science.aav9051

Marx, L., Niestrawska, J. A., Gsell, M. A. F., Caforio, F., Plank, G., and Augustin, C. M. (2022). Robust and efficient fixed-point algorithm for the inverse elastostatic problem to identify myocardial passive material parameters and the unloaded reference configuration. *J. Comput. Phys.* 463, 111266. doi:10.1016/j.jcp.2022.111266

MedlinePlus (2023). *Heart failure*. Bethesda (MD): National Library of Medicine. https://medlineplus.gov/heartfailure.html (Accessed July 10.

Moriz, A., Krieger, M., Gesenhues, J., Ketelhut, M., Mechelinck, M., and Hein, M. (2021). Non-linearity of end-systolic pressure-volume relation in afterload increases is caused by an overlay of shortening deactivation and the Frank-Starling mechanism. *Sci. Rep.* 11 (1), 3353. doi:10.1038/s41598-021-82791-3

Nakano, K., Sugawara, M., Ishihara, K., Kanazawa, S., Corin, W. J., Stewart, D., et al. (1990). Myocardial stiffness derived from end-systolic wall stress and logarithm of reciprocal of wall thickness. Contractility index independent of ventricular size. *Circulation* 82 (4), 1352–1361. doi:10.1161/01.cir.82.4.1352

Nielles-Vallespin, S., Khalique, Z., Ferreira, P. F., de Silva, R., Scott, A. D., Kilner, P., et al. (2017). Assessment of myocardial microstructural dynamics by *in vivo* diffusion tensor cardiac magnetic resonance. *J. Am. Coll. Cardiol.* 69 (6), 661–676. doi:10.1016/j.jacc.2016.11.051

Nikou, A., Dorsey, S. M., McGarvey, J. R., Gorman, J. H., Burdick, J. A., Pilla, J. J., et al. (2016). Computational modeling of healthy myocardium in diastole. *Ann. Biomed. Eng.* 44 (4), 980–992. doi:10.1007/s10439-015-1403-7

Noor, N., Shapira, A., Edri, R., Gal, I., Wertheim, L., and Dvir, T. (2019). 3D printing of personalized thick and perfusable cardiac patches and hearts. *Adv. Sci.* 6 (11), 1900344. doi:10.1002/advs.201900344

Nordsletten, D., McCormick, M., Kilner, P. J., Hunter, P., Kay, D., and Smith, N. P. (2011). Fluid–solid coupling for the investigation of diastolic and systolic human left ventricular function. *Int. J. Numer. Methods Biomed. Eng.* 27 (7), 1017–1039. doi:10.1002/cnm.1405

Palit, A., Bhudia, S. K., Arvanitis, T. N., Turley, G. A., and Williams, M. A. (2018). *In vivo* estimation of passive biomechanical properties of human myocardium. *Med. Biol. Eng. Comput.* 56 (9), 1615–1631. doi:10.1007/s11517-017-1768-x

Pezzuto, S. (2013). *Mechanics of the heart*. Phd dissertation, Politecnico di Milano.

Reichardt, M., Töpperwien, M., Khan, A., Alves, F., and Salditt, T. (2020). Fiber orientation in a whole mouse heart reconstructed by laboratory phase-contrast micro-CT. *J. Med. Imaging* 7 (2), 023501. doi:10.1117/1.JMI.7.2.023501

Rodriguez, D. A-A., Durand, E., de Rochefort, L., Boudjemline, Y., and Mousseaux, E. (2015). Simultaneous pressure-volume measurements using optical sensors and MRI for left ventricle function assessment during animal experiment. *Med. Eng. Phys.* 37 (1), 100–108. doi:10.1016/j.medengphy.2014.11.004

Sack, K. L., Dabiri, Y., Franz, T., Solomon, S. D., Burkhoff, D., and Guccione, J. M. (2018). Investigating the role of interventricular interdependence in development of right heart dysfunction during lvad support: a patient-specific methods-based approach. *Front. Physiology* 9, 520. doi:10.3389/fphys.2018.00520

Sagawa, K. (1978). The ventricular pressure-volume diagram revisited. *Circulation Res.* 43 (5), 677–687. doi:10.1161/01.res.43.5.677

Saltelli, A., Tarantola, S., Campolongo, F., and Ratto, M. (2004). *Sensitivity analysis in practice: a guide to assessing scientific models*. Wiley.

Sato, T., Shishido, T., Kawada, T., Miyano, H., Miyashita, H., Inagaki, M., et al. (1998). ESPVR of *in situ* rat left ventricle shows contractility-dependent curvilinearity. *Am. J. Physiology - Heart Circulatory Physiology* 274 (5), H1429–H1434. doi:10.1152/ajpheart.1998.274.5.H1429

Schwarzl, M., Ojeda, F., Zeller, T., Seiffert, M., Becher, P. M., Munzel, T., et al. (2016). Risk factors for heart failure are associated with alterations of the LV end-diastolic pressure-volume relationship in non-heart failure individuals: data from a large-scale, population-based cohort. *Eur. Heart J.* 37 (23), 1807–1814. doi:10.1093/eurheartj/ehw120

Shimizu, S., Dai, U., Kawada, T., Hayama, Y., Kamiya, A., Shishido, T., et al. (2018). Lumped parameter model for hemodynamic simulation of congenital heart diseases. *J. Physiological Sci.* 68 (2), 103–111. doi:10.1007/s12576-017-0585-1

Sommer, G., Schriefl, A. J., Andrä, M., Sacherer, M., Viertler, C., Wolinski, H., et al. (2015). Biomechanical properties and microstructure of human ventricular myocardium. *Acta Biomater.* 24, 172–192. doi:10.1016/j.actbio.2015.06.031

Sunagawa, K., Lowell Maughan, W., and Sagawa, K. (1983). Effect of regional ischemia on the left ventricular end-systolic pressure-volume relationship of isolated canine hearts. *Circulation Res.* 52, 170–178. doi:10.1161/01.res.52.2.170

Ten Brinke, E. A., Burkhoff, D., Klautz, R. J., Tschöpe, C., Schalij, M. J., Bax, J. J., et al. (2010). Single-beat estimation of the left ventricularend-diastolic pressure-volume relationship in patients with heart failure. *Heart* 96 (3), 213–219. doi:10.1136/hrt.2009.176248

Tiburcy, M., Hudson, J. E., Paul, B., Schlick, S., Meyer, T., Chang Liao, M. L., et al. (2017). Defined engineered human myocardium with advanced maturation for applications in heart failure modeling and repair. *Circulation* 135 (19), 1832–1847. doi:10.1161/CIRCULATIONAHA.116.024145

Witzenburg, C. M., and Holmes, J. W. (2017). "Biomechanics of myocardial ischemia and infarction," in *Biomechanics: Trends in modeling and simulation*. Editors G. A. Holzapfel, and R. W. Ogden (Cham: Springer), 233–269.

Zimmermann, W-H., Melnychenko, I., Wasmeier, G., Didié, M., Naito, H., Nixdorff, U., et al. (2006). Engineered heart tissue grafts improve systolic and diastolic function in infarcted rat hearts. *Nat. Med.* 12 (4), 452–458. doi:10.1038/nm1394